International Journal of Mechanical, Industrial and Aerospace Sciences
ISSN: 2517-9950
Vol:10, No:2, 2016

Numerical Simulation of Supersonic Gas Jet Flows and Acoustics Fields

Lei Zhang, Wen-jun Ruan, Hao Wang, Peng-xin Wang

***Abstract*—**The source of the jet noise is generated by rocket exhaust plume during rocket engine testing. A domain decomposition approach is applied to the jet noise prediction in this paper. The aerodynamic noise coupling is based on the splitting into acoustic sources generation and sound propagation in separate physical domains. Large Eddy Simulation (LES) is used to simulate the supersonic jet flow. Based on the simulation results of the flow-fields, the jet noise distribution of the sound pressure level is obtained by applying the Ffowcs Williams-Hawkings (FW-H) acoustics equation and Fourier transform. The calculation results show that the complex structures of expansion waves, compression waves and the turbulent boundary layer could occur due to the strong interaction between the gas jet and the ambient air. In addition, the jet core region, the shock cell and the sound pressure level of the gas jet increase with the nozzle size increasing. Importantly, the numerical simulation results of the far-field sound are in good agreement with the experimental measurements in directivity.

***Keywords*—**Supersonic gas jet, Large Eddy Simulation(LES), acoustic noise, Ffowcs Williams-Hawkings (FW-H) equations, nozzle size.

I. Introduction

THE supersonic jet noise, which is caused by the rapid mixing of the high speed gas and the surrounding relatively stationary medium, is one of the main features during rocket launching. The severe acoustic environment arising from the supersonic jet of the rocket engine induces serious damage to the surrounding staff and ground facilities, which has a certain potential risk for the reliability and safety of the rocket launching. Therefore, accurate prediction of the jet noise mechanisms is highly desired for suppressing the gas jet noise.

Anjaneyulu et al. [1] experimentally studied the acoustic characteristics of a heated supersonic jet under an ideally expanded condition. Accurate measurements of the mean flow structure of the jet using PIV were firstly proposed. Subsequently, the acoustic near-field and far-field measurements were made in an anechoic facility under the aforementioned operating conditions. Moreover, Peng [2] carried out an experiment to measure rocket noise by using microphones, and the results were analyzed by the LMS SCADAS. They found that the peak of the sound pressure level decreased with the propellant temperature increased, while an increase in the peak of the sound pressure level with the increase of the chamber pressure and the nozzle outlet Mach number was observed.

As the gradual improvement of the computing abilities, numerical techniques are becoming more and more attractive. The prediction of aerodynamic noise has caused the emergence of the computational aeroacoustics (CAA). Bailly and Bogey [3] summarized a review of the progress in the computational aeroacoustics theories and discussed connections between CFD and CAA using hybrid methods [4]-[10]. Bodony and Lele [11] made a survey of numerical methods used to predict the jet noise by LES. In the available simulations, the Kirchhoff surface integral method was used to project the mid-acoustic field onto the acoustic far-field. Depuru and Dowling [12] investigated numerically the acoustic sources and far-field noise of chevron and round jets. The acoustic sources were described by the fourth-order space-time velocity cross correlations, which were calculated in terms of a large-eddy simulation flow-field. In [13], a hybrid RANS-ILES approach was applied to simulate cold jet flows from a serrated nozzle at Mach number 0.9 and Reynolds number 1.03×10^6. The FW-H integral was used for the computation of far-field sound based on the near field LES data. The study showed the wider spectra had been obtained by using mesh refinement strategies. Sipatov et al. [14] developed a numerical method for the simulation of the jet noise by means of ANSYS-Fluent software. They fully analyzed the influences of various nozzles geometry features on the nozzles acoustic performance.

The gas jet noise is not only related to Mach number and Reynolds number, but also influenced by the nozzle size. In this paper, a hybrid method combining advanced CFD technology with an acoustic analogy, which has been used as a powerful tool to study the nozzle gas jet noise. Based on this method, the influences of the nozzle size on distribution characteristics of the jet flow field and the sound field are discussed in details.

II. Theoretical Models

A. Physical Model

Fig. 1 shows the shock structure of the jet flow-field. Owing to the viscous and turbulent of the nozzle exhaust plume, the mass and momentum are exchanged between the gas jet and the surrounding medium in the flow process. Because the surrounding medium is constantly involved in the jet flow field, the potential core of the jet (triangle region) is formed at the nozzle exit. Large and small eddies are formed in the shear

Lei Zhang, is with the School of Energy and Power Engineering, Nanjing University of Science and Technology, Nanjing, 210094, Jiangsu, China (e-mail: 13770568711@163.com).

Wen-jun Ruan and Hao Wang are with the School of Energy and Power Engineering, Nanjing University of Science and Technology, Nanjing, 210094, Jiangsu, China.

Peng-xin Wang is with the China Baicheng Weapon test centre，Baicheng 137001, Jilin, China.

layer of the gas jet. These eddies are very small in size near the nozzle exit where they originally form, and then they become larger as their propagating along the plume until they eventually dissipate. Ultimately, the formation, propagation and dissipation of eddies result in the jet noise.

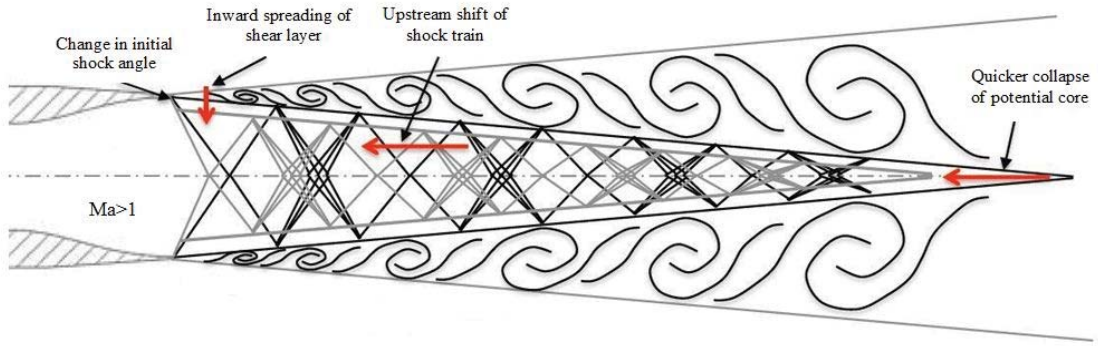

Fig. 1 Schematic of the structure of fluidic injection [15]

Fig. 2 shows a simulation model of nozzle configuration. In Fig. 2, D_t and D_e denote the nozzle throat diameter and the nozzle exit diameter respectively. The gas jet flows across the nozzle, and achieves the required Mach number at the nozzle exit. For the three designed nozzles, the designed exit Mach number is 2. The nozzle geometry parameters are given in Table I.

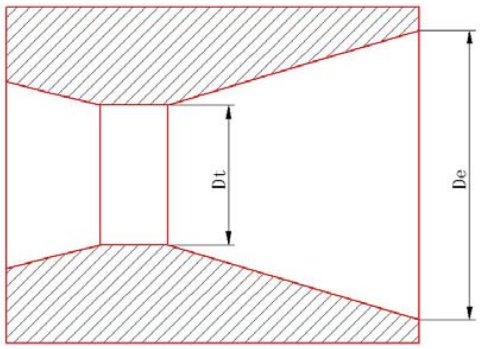

Fig. 2 Structural schematic of the nozzle

TABLE I
THE GEOMETRIC PARAMETERS OF NOZZLE

Nozzle	D_t/mm	D_e/mm
1	8	10.4
2	10	13
3	12	15.6

B. Basic Conservation Equations

The three dimensional Favre filtered conservation equations of continuity, momentum and energy are employed, which can be written as:

$$\frac{\partial \bar{\rho}}{\partial t}+\frac{\partial(\bar{\rho}\tilde{u}_i)}{\partial x_i}=0 \tag{1}$$

$$\frac{\partial(\bar{\rho}\tilde{u}_i)}{\partial t}+\frac{\partial(\bar{\rho}\tilde{u}_j\tilde{u}_i)}{\partial x_j}+\frac{\partial \bar{p}}{\partial x_i}=\frac{\partial(\tilde{\tau}_{ij}-\tau_{ij}^{SGS}+D_{ij}^{SGS})}{\partial x_j} \tag{2}$$

$$\frac{\partial(\bar{\rho}\tilde{E})}{\partial t}+\frac{\partial[(\bar{\rho}\tilde{E}+\bar{p})\tilde{u}_i]}{\partial x_i}=\frac{\partial}{\partial x_i}(-\tilde{q}_i+\tilde{u}_j\tilde{\tau}_{ij}+J_i^{SGS}+\sigma_i^{SGS}-Q_i^{SGS}-H_i^{SGS}) \tag{3}$$

with

$$\tilde{\tau}_{ij}=2\tilde{\mu}\tilde{S}_{ij}-\frac{2}{3}\tilde{\mu}\delta_{ij}\tilde{S}_{kk} \tag{4}$$

$$\tilde{q}_i=-\frac{\tilde{\mu}C_p}{\mathrm{Pr}}\frac{\partial\tilde{T}}{\partial x_i} \tag{5}$$

where the overbar and the tilde denote the spatial filter and the Favre filter respectively, i.e. $\tilde{f}=\overline{\rho f}/\bar{\rho}$. ρ, u_i, p, E represent the density, velocity component, pressure and specific total energy, respectively. μ is the molecular. C_p is the constant -pressure specific heat. Pr is the Prandtl number. The subgrid closure terms (τ_{ij}^{SGS} D_{ij}^{SGS} J_i^{SGS} σ_i^{SGS} Q_i^{SGS} H_i^{SGS}) are given in [16]. Dynamic Smagorinsky's model is used to describe subgrid stresses. The state equation of the perfect gas and the Sutherland's law for the molecular viscosity coefficient μ are employed.

C. The Ffowcs Williams and Hawkings Model

The Ffowcs Williams and Hawkings (FW-H) integral is solved numerically to determine acoustic signals at R=2m from the nozzle exit center at the polar angle θ, which is defined as the angle between the jet axis and the observer line R. The FW-H equation can be expressed as:

$$\frac{1}{c^2}\frac{\partial^2 p'(x,t)}{\partial t^2}-\nabla^2 p'(x,t)=\frac{\partial^2}{\partial x_i\partial x_j}\left[T_{ij}H(f)\right]-\frac{\partial}{\partial x_i}\left[L_i\delta(f)\right]+\frac{\partial}{\partial t}\left[(\rho_0 U_i)\delta(f)\right] \tag{6}$$

with

$$U_i=[1-(\rho/\rho_0)]v_i+\rho u_i/\rho_0 \tag{7}$$

$$L_i=P_{ij}n_j+\rho u_i(u_n-v_n) \tag{8}$$

$$T_{ij}=\rho u_i u_j+P_{ij}-c^2(\rho-\rho_0)\delta_{ij} \tag{9}$$

where p' is far-field sound pressure. T_{ij} is the Lighthill stress tensor. $H(f)$ is Heaviside function. $\delta(f)$ is Dirac delta function. P_{ij} is the compressive stress tensor. ρ_0 is the constant reference density. u, v and c are fluid velocity, body surface velocity and velocity of sound, respectively.

The first term on the right side of (6) is a quadrupole source caused by unsteady shear stresses. The second term is a dipole source by unsteady external forces. The third term is a monopole source caused by unsteady mass injection. When the high speed gas ejects into the stationary air, a large number of vortices are generated due to the turbulence. The stress tensor in the first term on the right side of (6) is correspondingly changed, and the quadrupole radiation source is generated. Therefore, the main sound source of the rocket gas jet noise is the quadrupole.

D.Initial and Boundary Conditions

Fig. 3 shows the computational domain, which includes both the nozzle geometry and the plume region. The length of the domain is about $50D_e$; its radial size is about $30D_e$. The parameter values of the air medium are the initial conditions of the computational domain. The boundary of the nozzle is a fixed wall, and its exit is connected with the atmosphere. The parameter values of the nozzle inlet are inlet boundary condition of the computational domain. The values of the initial and inlet boundary conditions are shown in Table II. The sound source surface is constructed in the flow field area, and it is assigned an interior boundary. Fig. 4 shows the gird model of the computational domain.

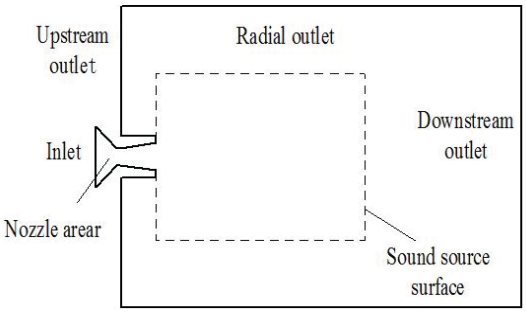

Fig. 3 Computational domain and boundary conditions

TABLE II
THE INITIAL AND BOUNDARY CONDITIONS

	P(MPa)	T(K)
Initial conditions	0.101	300
Inlet boundary conditions	1	3000

III.RESULTS AND DISCUSSION

A. Flow Field Results

Fig. 5 shows the velocity distribution of the gas jet under different nozzle sizes, which are characterized by complex shock and expansion wave interactions. It can be seen from Fig. 5 that a Prandtl-Meyer expansion follows the flow at the nozzle exit, causing a significant increase in the velocity of the gas jet. The existence of the compression waves could be attributed to the expansion waves reflect from the pressure free boundary. Periodic shock cell structures are formed in the plume of the under-expanded jet, among three conditions of the jets. These shock structures are consistent with the supersonic jet flows. The downstream shocks are weakened due to the momentum dissipation of the gas jet. Typically, the initial cell length of the gas jet and the jet range increase as the nozzle size increasing, which results in small amounts of air entering the mixing layer from the atmosphere.

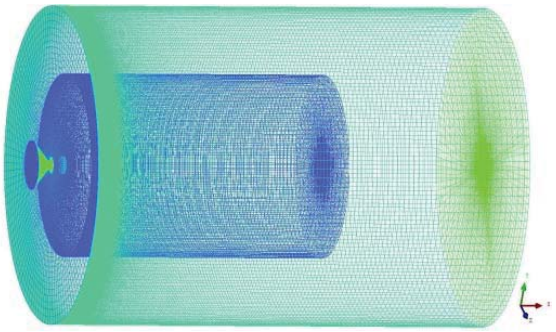

Fig. 4 The grid model of computational domain

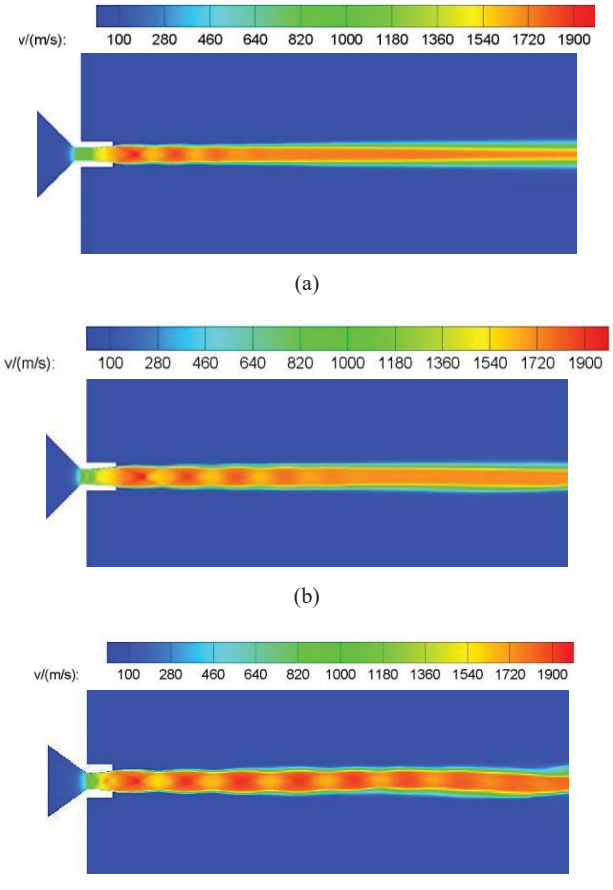

Fig. 5 The velocity distribution of supersonic jet *(a) D_e=10.4mm,* (b) D_e=13mm, (c) De=15.6mm

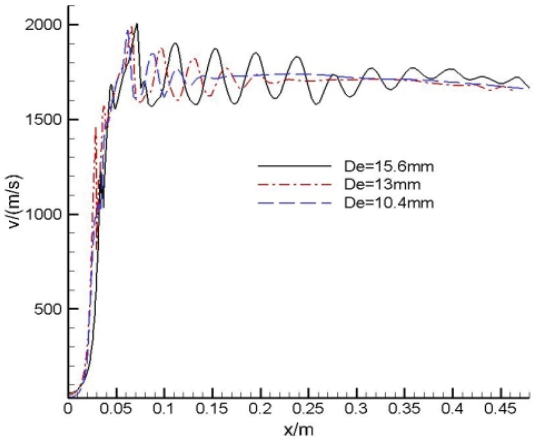

Fig. 6 Centerline velocity of supersonic jet

Fig. 6 shows the velocity curves over distance on the central axis of the gas jet under different nozzle sizes. As can be seen from the figure, it clearly shows the effects of the nozzle size on the jet core regions. With the increase of the nozzle size, the dramatic change in the velocity fluctuations is noted at the near nozzle exit region. These fluctuations in the velocity are attributed to the periodic shock structures as seen in Fig. 5.

Fig. 7 shows the pressure curves over distance on the central axis of the gas jet under different nozzle sizes. With the increase of the nozzle sizes, a greater amplitude and longer duration in fluctuations of the pressure can be observed. From Fig. 7, one can also see that the over trend of the curves is very much similar to that of Fig. 6.

The *x*-axis at x=0 corresponds to the nozzle inlet. At axial location of x=0.2 m, the velocity curves along the radial direction is shown in Fig. 8. The centerline velocity is the largest along the radial direction. The velocity remains almost constant in the core region, whereas it drops sharply in the jet shear layer. In addition, the core region increases along the radial with the increase of the nozzle size. These analyses are consistent with the jet dynamics.

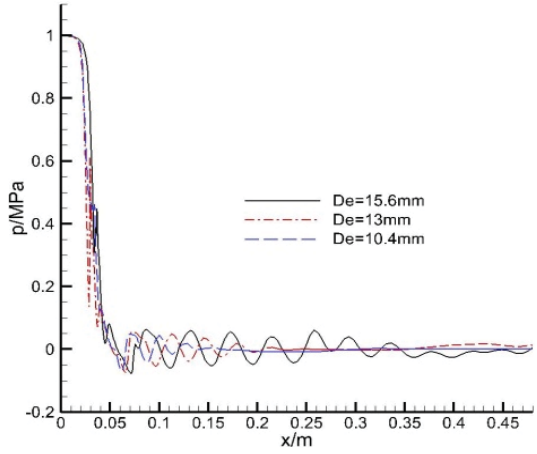

Fig. 7 Centerline pressure of supersonic jet

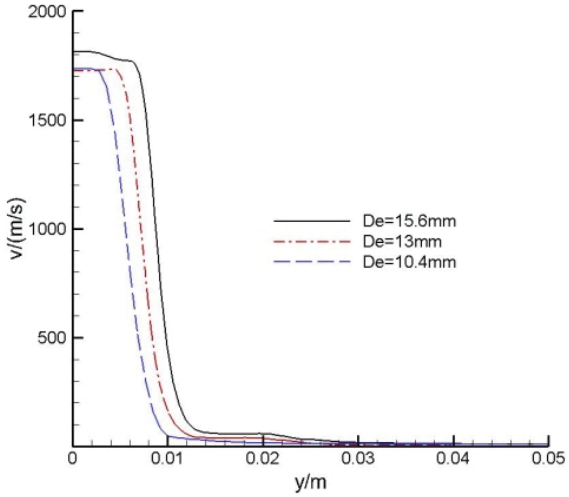

Fig. 8 Velocity distribution along the radial at x=0.2m

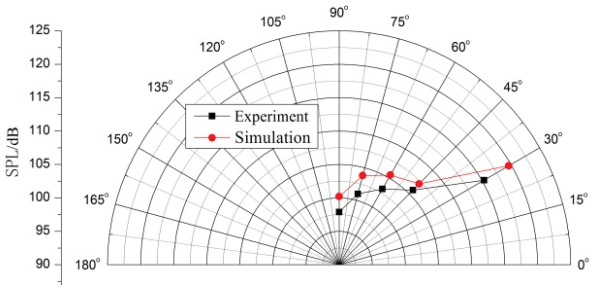

Fig. 9 Comparison of the predicted SPL with experiment

B. Acoustics Results

Fig. 9 shows the sound pressure level (SPL) of the jet noise when the diameter of nozzle exit is D_e=10.4mm. As can be seen from the figure, the maximum value of the sound pressure level appears at the polar angle θ=30º, which indicates that the dominant noise is radiated near this angle. There is a good agreement between predictions and measurements [2] for the sound pressure level directivity. However, the sound pressure levels seem to be over-predicted about 3dB in the present prediction, compared with the experimental results. These results are consistent with previous study [8]. Finer grids are used to test the grid independence. The numerical results on SPL between different grid resolutions are little different and only have an estimated maximum error of 2%.

The directivity of the sound pressure level of the jet noise under different nozzle sizes are shown in Fig. 10. The sound pressure level decreases with the polar angle θ increasing under the same nozzle size. The SPL at the polar angle θ=90º is almost 20dB lower than that at θ=30º. The sound waves do not propagate uniformly in all directions due to refraction by the gas jet. As can be seen from Fig. 10, the sound pressure levels increase as the nozzle size is bigger at the same polar angle. The result can be explained as follows: greater pressure fluctuations and more intense turbulent occurred with the increase of nozzle size, thereby resulting to the extension in

the jet core region. In conclusion, the acoustic radiation is related to the characteristic of jet flow.

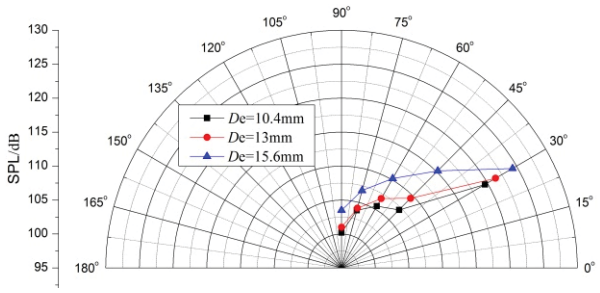

Fig. 10 Effect of the nozzle size on the jet noise

IV. Conclusions

Base on the results of the numerical simulation, the following conclusions can be obtained:

(1) A domain decomposition approach for calculating the coupling of jet flow and acoustic is used to simulate the supersonic jet noise. The flow domain is calculated by LES using a Finite Volume method with structured grids, while the acoustic one is performed using the FW-H integral. The numerical simulation results are in a good agreement with the experimental data of the sound pressure level in the far-field.

(2) The calculation results reasonably capture the salient flow feature, such as the expansion waves, compression waves and the jet shear layer, etc., which are generated in the under-expanded jet flow. When the nozzle size becomes bigger and expansion ratio remain unchanged, the shock reflection distance is longer, and a greater amplitude and longer duration in fluctuations of the velocity and pressure is observed. Therefore, the changes of the major flow features significantly affect the jet downstream in a larger region.

(3) The supersonic jet noise is relevant to the nozzle size. The sound pressure levels will increase with larger nozzle size because of the increased shock strength and turbulence levels near the nozzle exit. The maximum value of the sound pressure level appears at the polar angle $\theta=30^{o}$. In addition, the sound waves do not propagate uniformly in all directions owing to refraction by the gas jet.

References

[1] Anjaneyuiu K, Brenton G, David W. Aeroacoustics of a heated Mach 2.0 jet. AIAA 2005-2931.
[2] Peng XB, Li JM, Hu, CB. Experimental study on jet noise characteristics of solid rocket motor. Journal of Experiments in Fluid Mechanics. 2013;27(1):52~55 (in Chinese).
[3] Bailly C, Bogey C. Contributions of computational aeroacoustics to jet noise research and prediction. Int J Comput Fluid Dyn 2004;18(6):481-91.
[4] Cunha G, Redonnet S. Towards a robust and accurate CFD/CAA coupling procedure for hybrid methods in aeroacoustics, Part 1: on the optimization of CFD/CAA coupled calculations. AIAA;2012-2063.
[5] Mathieu L, Franck C. Analysis of noise radiation mechanisms in hot subsonic jet from a validated large eddy simulation solution. Physics of Fluids 2015;27(7).
[6] Papamoschou D, Morris PJ, Mclaughlin DK. Beamformed flow-acoustic correlations in a supersonic jet. AIAA J 2010; 48(10):2445-2453.
[7] Morris PJ, Mclaughlin DK, Kuo CW. Noise reduction in supersonic jets by nozzle fluidic inserts. J sound and vib 2013, 332:3992-4003.
[8] Koh S, Schroder W, Meinke M. Noise sources in heated coaxial jets. Computers&Fluids 2013; 78:24-28.
[9] Koh S, Schroder W, Meinke M. Turbulence and heat excited noise sources in single and coaxial jets. J Sound Vib 2010; 329:786-803.
[10] Fu DB, Yu Y, Niu QL Simulation of underexpanded supersonic jet flows with chemical reactions. Chinese Society of Aeronautics and Astronautics 2014, 27(3):505-513.
[11] Bodony D, Lele SK. Current status of jet noise predictions using large-eddy simulation. AIAA J 2008;46(2).
[12] Depuru NK, Dowling AP. Acoustic sources and far-field noise of chevron and round jets. AIAA J 2015;53(9).
[13] Xia H, Tucker PG. Numerical simulation of single-stream jets from a serrated nozzle. Flow Turbulence Combust 2012, 88:3-18.
[14] Sipatov AM, Usanin MV, Chuhlantseva NO. Applying fluent software for jet noise generation modeling. AIAA 2010-3843.
[15] Daniel C, Bhupatindra M. The response of supersonic jet noise components to fluidic injection parameters. AIAA 2013-2196.
[16] Xu CY, Chen LW, Lu XY. Large-eddy simulation of the compressible flow past a way cylinder. J. Fluid Mech. 2010; 665:238-273.